Alternating Bias Assisted Annealing of Amorphous Oxide Tunnel Junctions

D. P. Pappas, ^{1,*} M. Field, ¹ C. Kopas, ¹ J. A. Howard, ¹ X. Wang, ¹ E. Lachman, ¹ Lin Zhou, ^{2,3} Jinsu Oh, ^{2,3} K. Yadavalli, ¹ E. A. Sete, ¹ A. Bestwick, ¹ M.J. Kramer, ^{2,3} and J. Y. Mutus ¹

¹Rigetti Computing, 775 Heinz Avenue, Berkeley, CA 94710, USA

²Ames National Laboratory, Ames, IA 50011, USA

³Department of Materials Science and Engineering, Iowa State University, Ames, IA 50011, USA

(Dated: January 17, 2024)

We demonstrate a transformational technique for controllably tuning the electrical properties of fabricated thermally oxidized amorphous aluminum-oxide tunnel junctions. Using conventional test equipment to apply an alternating bias to a heated tunnel barrier, giant increases in the room temperature resistance, greater than 70%, can be achieved. The rate of resistance change is shown to be strongly temperature-dependent, and is independent of junction size in the sub-micron regime. In order to measure their tunneling properties at mK temperatures, we characterized transmon qubit junctions treated with this alternating-bias assisted annealing (ABAA) technique. The measured frequencies follow the Ambegaokar-Baratoff relation between the shifted resistance and critical current. Further, these studies show a reduction of junction-contributed loss on the order of $\approx 2 \times 10^{-6}$, along with a significant reduction in resonant- and off-resonant-two level system defects when compared to untreated samples. Imaging with high-resolution TEM shows that the barrier is still predominantly amorphous with a more uniform distribution of aluminum coordination across the barrier relative to untreated junctions. This new approach is expected to be widely applicable to a broad range of devices that rely on amorphous aluminum oxide, as well as the many other metal-insulator-metal structures used in modern electronics.

I. INTRODUCTION

The preparation of amorphous thin film materials is surprisingly simple and devices based on them are ubiquitous in electronics, but their morphology is surprisingly complex and challenging to control. Among other similar materials, amorphous aluminum oxide tunnel (a-AlO_x) junctions stand out due to their importance in both cryogenic and room temperature devices. Applications range from those that utilize the Josephson effect [1], such as SQUID magnetometers [2], superconducting qubits [3, 4], amplifiers [5, 6], RSFQ logic [7], to room temperature magnetic tunnel junctions and memory elements [8–10].

Due to the cryogenic application of these oxide barriers for Josephson junctions, we can probe not only their resistance but also the prevalence of defects and loss using superconducting qubits. This is especially relevant to the field of quantum information since a-AlO_x is a key ingredient in transmon qubits [13], the invention of which has fueled much of the rapid development of superconducting applications research over the past decade. The junction properties are crucial in the overall properties and performance of the qubit. Most importantly, the critical current, I_c of the barrier sets the Josephson energy of the device, $E_J = I_c \Phi_0 / 2\pi$, where Φ_0 is the flux quantum, which determines the parameters such as the frequency, anharmonicity, and charge noise sensitivity. Specifically, I_c can be predicted by the Ambegaokar–Baratoff formula, i.e. $I_C = \pi \Delta/2eR_n$ [14], where, the variables R_n and Δ

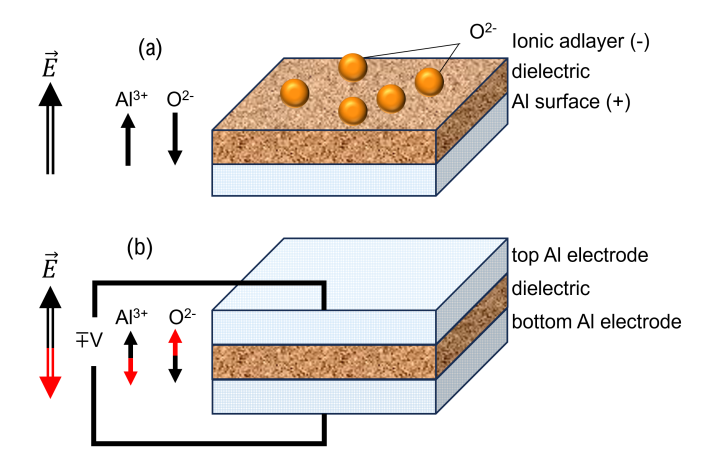


FIG. 1. (a) Oxide growth on aluminum according to the Cabrera-Mott mechanism [11, 12]. The primary assumption is that electrons can freely ionize adsorbed oxygen. This leads to a relatively low voltage, $V_{\rm Mott} \sim 1 \rm V$, that creates a strong electric field in the thin oxide. Aluminum cations and oxygen anions at the surfaces and in the barrier feel opposite forces due to this field and exchange places, mediated by vacancy motion. (b) Method of mixing the ${\rm Al/AlO}_x/{\rm Al}$ trilayer by applying alternating voltages, on the order of magnitude of $V_{\rm Mott}$ but less than the dielectric breakdown voltage [10], between the two plates. This applies alternating and opposing forces on the two species.

are the resistance of the junction (in its normal state) and the superconducting gap of the electrodes.

Unfortunately, while it is essential that I_c , and hence R_n , is well defined, a large spread of R_n in nominally identical junctions is typically observed, on the order of 5-10% at the wafer level [15]. This is due to both intrin-

^{*} dpappas@rigetti.com

sic properties and extrinsic effects. Intrinsic issues include the exponential dependence of the tunneling on the thickness [16]; grain structure; and interface roughness. Extrinsic effects arise from the effects of lithography uncertainties [17], processing, electrostatic sensitivity, and circuit design.

Moreover, the amorphous nature of the oxide layer results in the inclusion of defects that can cause two-level systems (TLS's) near the qubit frequency that typically reduce coherence, or the defects can result in two-level fluctuators (TLF's) at very low frequencies that push the qubit frequency around [18, 19].

The default method of making junctions, also used in this work, employs thermal oxidation of an aluminum surface described by the Cabrera-Mott model which shows the initial oxidation is driven by an intrinsic electric field [11, 12]. This process is convenient and powerful because it is conformal and self-limiting in thickness. In the thin-barrier limit the formation of the oxide barrier is governed by drift-dominated atomic diffusion [12, 20] of the charged constituent elements, Al³⁺ and O²⁻, in opposite directions, as illustrated in Fig. 1 (a). This diffusion is driven by the strong E-field ~ 1 GV/m generated by the adsorbed ionic ad-layer. In these, and other metal-insulator-metal oxides, the relevant parameter is referred to as the Mott voltage, $V_{\rm Mott} \approx 0.5$ -1 V for aluminum oxide [21].

There have been many efforts to improve the properties of the a- AlO_x material, focused primarily on understanding and optimizing the junction formation and post-processing, i.e. pressure, time, [22], interface preparation, etches, simulations, etc., see Ref. [23, 24] and citations therein. These efforts have met with limited success, and it is typically assumed that the properties of the junctions, as formed, are relatively frozen-in and difficult to adjust. For example, annealing the junctions to high temperatures can slightly change the resistance, globally heating many junctions has limited efficacy due to nanoscopic morphology differences of nominally identical junctions at the domain and atomic level. Since the resistance tends to increase on continued annealing, novel approaches to sequentially targeting the junctions have been useful in mitigating these spreads by targeting a slightly lower resistance than desired and then heating the individual junctions locally to bring them into tolerance [25–27]. However, these procedures involve the addition of optical elements to the test and measurement apparatus and appear to be limited to adjustments of the resistances up to about 10-12\%, i.e. on the order of the junction spread. This limits the number of junction arrays that can be successfully adjusted, based on the initial distribution of the junctions.

On the other hand, it has been shown that oxidation can be enhanced by an external voltage [28], for example, that generated by e-beam bombardment at the surface [29]. When comparing with other physical material systems, e.g. magnetic [30] and piezo-electric [31], where annealing while applying an alternating field polarity can

have significant positive effects, this approach has not yet been investigated in connection to a-AlO_x tunnel junctions and is illustrated in Fig 1(b).

II. EXPERIMENTAL SETUP AND RESULTS ON JUNCTIONS

In this work, we have investigated this approach in a protocol that we refer to as alternating bias-assisted anneal (ABAA). The ABAA technique entails applying an alternating polarity voltage pulse train to the junctions during a global, low-temperature anneal. ABAA can be implemented using a conventional probe station with a low-temperature heating stage, as illustrated in Fig. 2. Using this technique, it can be expected that the Al^{3+} cations and O^{2-} anions in the barrier will be driven in opposite directions at each pulse. By alternating the bias voltage the ions can be driven out of local, metastable sites into a lower energy configuration. In general, the guidelines used for the voltage profiles were that it should be on the order of V_{Mott} and less than the breakdown voltage, $V_B \sim 1.5$ V [10, 21]. When considering the time duration of the pulse, we note that by staying well below V_B the junction properties were observed to evolve relatively slowly, on the order of 100's of seconds, similar to the known oxidation rates of these surfaces. Finally, a relatively low temperature is desired to not expose junctions to a higher temperature than the highest temperature they are exposed to during the fabrication process.

The equipment and pulse sequences used for the tuning consist of a standard source-measure unit (SMU) and a probe station with a heated platen, illustrated in Fig. 2(a,b). The SMU was programmed to provide a train of 1-second-long anneal-assist pulses after the wafer was brought to the target temperature. The pulse amplitudes were set in the range of 0.8 - 1.1 V. The resistance of the junctions was measured after each pulse with an additional pulse at low voltage. As shown in Fig. 2(d), when unipolar pulse trains were applied to the junctions a relatively small change in the resistance was observed. Changes of about 2% and 6%, respectively, were registered for negative-only and positive-only voltages after about 200 pulses. However, when alternating-polaritybias (AB) pulses were used, as illustrated in Fig. 2(c), resistance changes of more than 70% were recorded as shown in Fig. 2(d). In addition, we note two new features of the ABAA process that we address later in this paper: first, that a cyclic response was typically observed for the AB pulse trains, as illustrated in the Fig. 2(d) inset; and second, a systematic jump in the resistance curve typically occurs during the process.

Further studies including the temperature dependence of this effect are shown in Fig. 3. We find the rate increases significantly as the temperature is increased from 25 up to 80°C. The increase is on the order of $2\times$ every 10°C, consistent with that expected from an Arrhe-

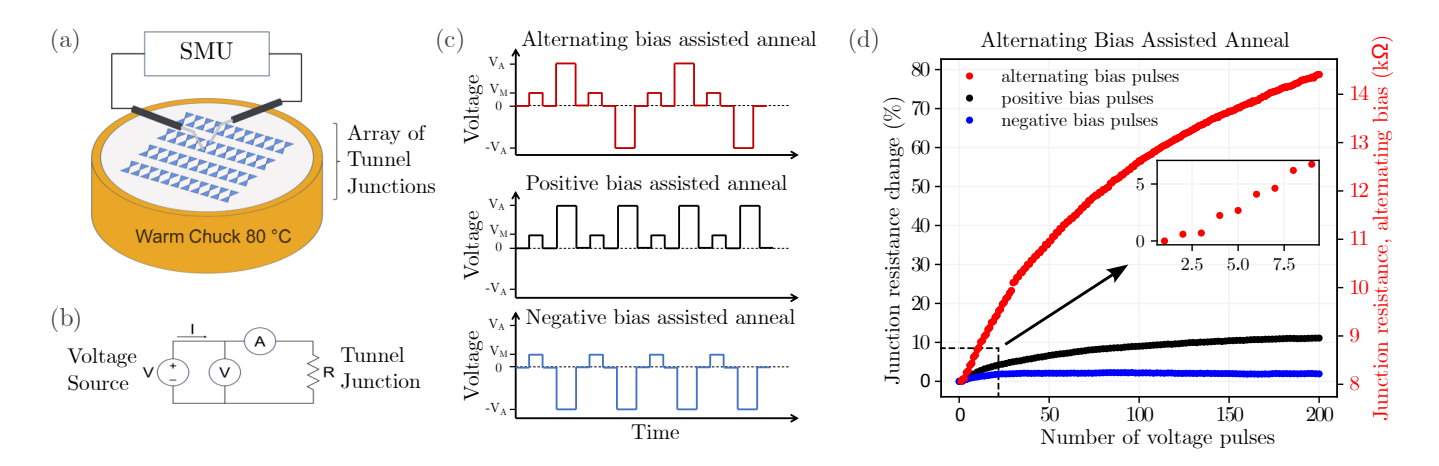


FIG. 2. Schematic diagram of the bias schemes used to anneal tunnel junctions. (a) A block diagram of the apparatus. In all cases, the voltage source has the positive terminal connected to the top electrode and the negative terminal connected to the bottom electrode sitting on the substrate. (b) A circuit diagram. (c) Bias pulses at V_A are applied for 1 second. In this paper $V_A = 0.9$ V. Between the bias pulses a low measurement pulse of $V_M = 10$ mV is used to measure the low bias resistance of the junction. (d) Data for voltage-assisted annealing using alternating bias assisted anneal (ABAA) at 80°C vs. unipolar (positive and negative w.r.t. the top electrode) voltage pulses. The maximum voltage amplitude $V_A = \pm 0.9$ V with a 1-second pulse length. The area of the junction under test is 1.55 μ m × 0.24 μ m = 0.37 (μ m)². The inset is a zoom in on the start of the ABAA process and shows the cyclic change in junction resistance with a repeated sequence of small and large resistance changes when applying alternating bias bipolar pulses.

nius law. On the other hand, the size dependence (not shown) is flat over more than an order of magnitude, indicating that the mechanism is not due to the perimeter or other side effects. This points to local effects such as reordering and increased coordination of the atoms in the

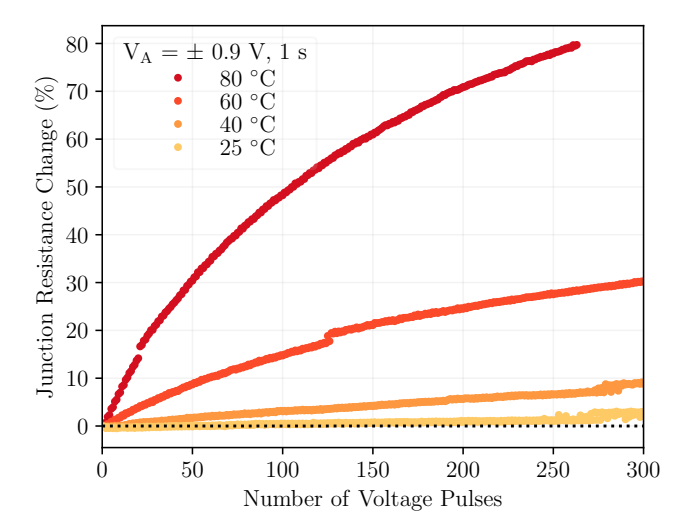


FIG. 3. Junction resistance change as a function of the number of AB pulses for four nominally identical junctions from the same wafer at different substrate temperatures. In addition to the relatively smooth increase in junction resistance as the AB pulses are applied, resistance jumps are observed for each device, sometimes appearing as a random telegraphic switching of resistance that settles at the higher resistance value.

barrier, leading to changes in the effective barrier height as atoms reach a more stable configuration or interfacial modifications such as smoothing or thickening of the barrier. Furthermore, since the data was taken at constant voltage, we infer that it is not a current-driven diffusion effect. This has more practical implications from the perspective of SQUID-based devices, such as sensors and tunable qubits, because these devices are typically made using two parallel circuits with junctions that may or may not be the same size. Finally, we note that the resistance jumps are also evident in the 25, 40, and 60°C data.

III. EFFECT OF ABAA ON TRANSMON QUBITS

We probe the effect of ABAA on the tunneling properties of the barrier by characterizing transmon qubits taken from the same wafer with and without ABAA. We measure a variety of properties associated with the junctions: whether I_C follows the behavior expected by the Ambegaokar-Baratoff relationship, the impact of the barrier on qubit loss, and the presence of strongly coupled TLS's. We measured both tunable and fixed-frequency qubits [32]. For this test, we select 5 equivalent chips. Two chips containing 16 qubits each were treated with ABAA. Of these, 24 qubits had AB voltage pulses applied (3 qubits failed to a short circuit, 8 tunable qubits lost tunability), while 8 qubits on the same chip were not subjected to AB voltage pulsing, and one of these was not measurable. These devices were characterized contemporaneously with another reference set of one chip heated to

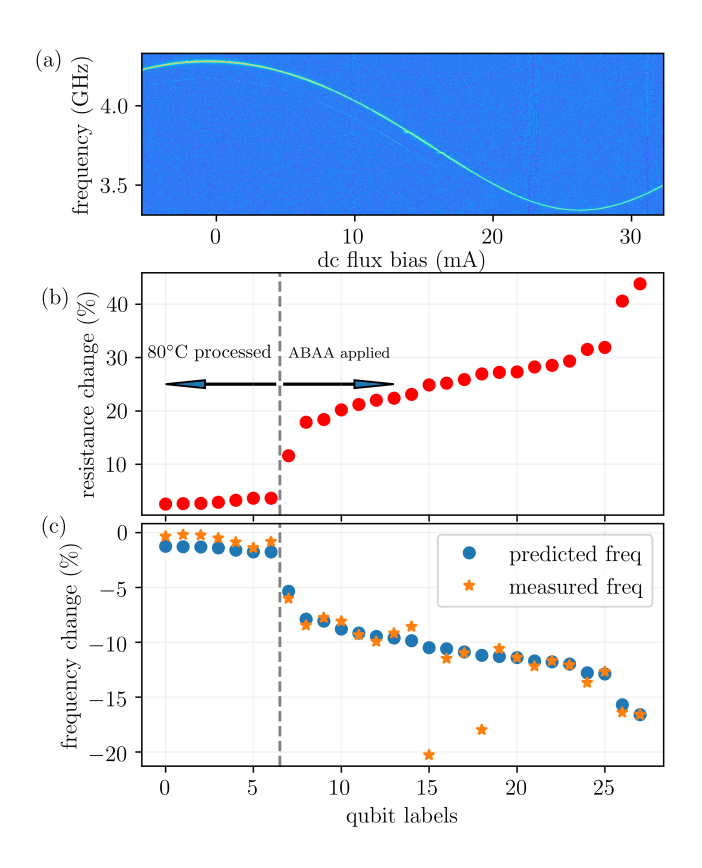


FIG. 4. Summary of qubit characterizations. (a) A spectrum of a tunable qubit that has been treated with ABAA. (b) Measured junction resistance shift (red dots) resulting from the ABAA trimming of junctions. (c) The blue dots show the predicted frequency change from untreated values using the Ambegaokar-Baratoff relation while the orange stars show the measured frequency change.

80°C for 1 hour to mimic ABAA processing (16 qubits, one of which was not measurable), and two chips were not post-processed with annealing (32 qubits, 2 were not measurable).

The Ambegaokar-Baratoff parameter set for this ensemble was first determined using the untreated devices. Then the measured frequencies of the treated qubits were calculated for various resistance-trimming amounts. For the non-tunable qubits, this is straightforward, while for the tunable gubits, it is necessary to find the maximum frequency, i.e. zero flux-bias, point. This process is illustrated in Fig 4(a), showing the spectrum of a tunable qubit. The spectrum not only allows one to find the maximum frequency, but it also probes for the existence of any strongly coupled TLS in this frequency range. In fact, for this qubit and all of the other tunable devices in the ABAA ensemble, for a total tunability range of 5.4 GHz in 9 tunable qubits, we found no evidence of strongly coupled TLSs. Measurements on reference gubits that did not receive any additional processing, and those that were heated to 80°C but not ABAA processed have 0.7 TLS/GHz and 0.6 TLS/GHz, respectively. Furthermore,

TABLE I. Qubit coherence for ABAA treated, 80 °C annealed and unprocessed qubits. The error bars are 1σ standard deviations.

Qubit Coherence			
ABAA treated	28.4 ± 8.7	34.1 ± 10.6	62.5 ± 23.1
80 °C annealed	20.9 ± 4.6	29.0 ± 12.7	37.9 ± 39.9
ABAA treated 80 °C annealed Unprocessed	19.5 ± 5.0	22.7 ± 12.3	41.4 ± 45.1

the low-frequency stability of one of the devices was monitored over many hours and there was no evidence of coupling to TLFs [19].

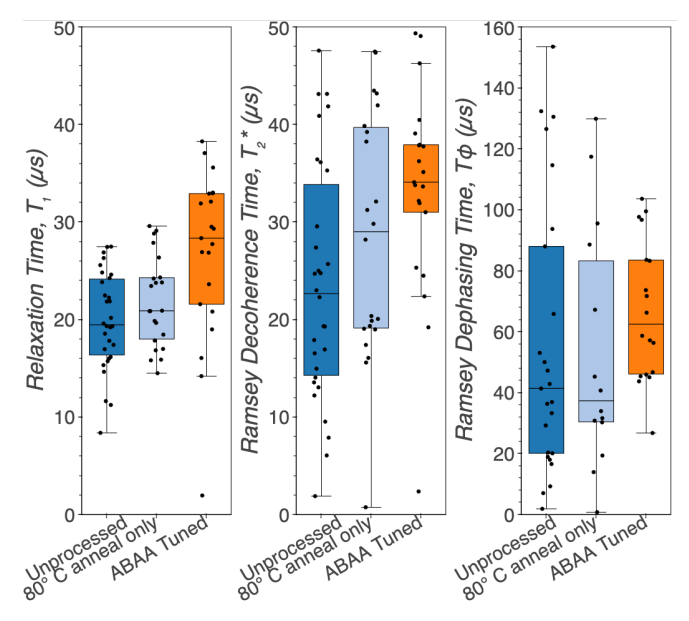


FIG. 5. Summary of qubit lifetimes. (a): Qubit relaxation time, (b): Qubit Ramsey decoherence time, and (c) Qubit dephasing time for three populations of qubits: unprocessed, annealed to 80 °C, and tuned using ABAA with $V_A = 1$ V, 1 s and T = 80°C. The number of measured qubits in the Unprocessed data set is $n_{\rm qubit} = 30$, the 80°C anneal only set has $n_{\rm qubit} = 22$, and the ABAA tuned set has $n_{\rm qubit} = 21$.

In Figure 5 we show coherence metrics for all qubits measured in the study. Here, each data point corresponds to the median of many measurements on one particular qubit. We observe that the ABAA processed devices have a higher median T_1 than both the unprocessed and the devices that were only heated to 80°C, although the T_2^* and T_ϕ values between sample sets are not distinguishable within the spread of the values, as shown in Table I.

When analyzing processes that may reduce loss in qubits, it is useful to compare these metrics in the form of a frequency-normalized loss tangent $(1/(T_1 \times (f_{01}));$ the ABAA tuned sample set has median loss tangent of 8.8×10^{-6} , while both the 80°C annealed and unprocessed sets have median loss tangents of 1.0×10^{-5} and 1.1×10^{-5} , respectively. We found that the coherence was typically improved after the ABAA process, indicating that the resistance trimming may have reduced the

median loss tangent in the junction by about 2×10^{-6} . Furthermore, the effects of the resistance trimming on the qubit frequencies are shown in Fig. 4(b), where we see that the increase of the resistance results in a reduced measured frequency, shown in Fig. 4(c) as orange stars. The expected frequencies (blue circles), compare well with the measured values. We also find the Ambegaokar-Baratoff relationship is consistent between junctions with ABAA applied vs. unprocessed with values of $(1.32\pm0.084)~{\rm pH}/\Omega$ and $(1.27\pm0.109)~{\rm pH}/\Omega$ respectively.

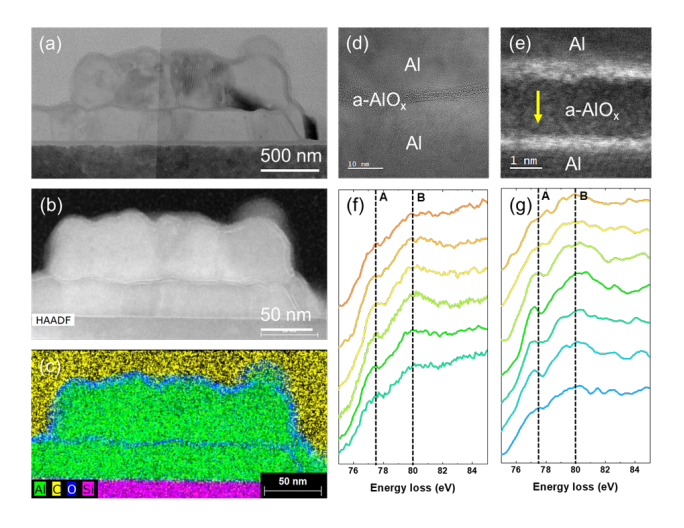


FIG. 6. Electron microscopy analysis on ABAA-treated junction. (a) a low-magnification cross-sectional TEM image of the junction. (b) a HAADF-STEM image and (c) a corresponding STEM-EDS elemental distribution map. (d) High-resolution TEM image of Al/a-AlO $_x$ /Al interfaces. (e) HAADF-STEM image of Al/a-AlO $_x$ /Al interfaces. (f) ELNES of Al23 edge of the ABAA-treated sample taken from the yellow arrow indicated region in (e), and (g) ELNES of Al23 edge of the untreated AlOx barrier from reference [33]

Finally, TEM imaging was employed to investigate morphological changes in the junctions due to the ABAA Secondary electron images for the JJ surface were acquired using a scanning electron microscope (SEM) (Helios, Thermo Fisher Scientific Ltd.) at 2 kV. Transmission electron microscope (TEM) samples were prepared by a focused ion beam instrument with a gas injection system (Helios, Thermo Fisher Scientific Ltd.). The TEM samples were thinned to electron beam transparency by a Ga⁺ ion beam from 30 to 2 kV. The TEM samples were investigated by an aberration-corrected TEM (Titan Cube, Thermo Fisher Scientific Ltd.) at 200 kV. A high-angle annular dark-field (HAADF) detector was used for dark-field imaging in scanning TEM (STEM) mode with a convergent semi-angle and a collection semi-angle of 18 mrad and 74-200 mrad, respectively. Energy-dispersive X-ray spectroscopy (EDS) and electron energy-loss spectroscopy (EELS) studies were carried out with probe currents of 250 nA and 50 nA,

respectively. Dual EELS was performed to acquire allelectron energy-loss (ELL) spectra. The plural scattering effect of all the raw ELL spectra was removed via Fourier-ratio deconvolution.

TEM imaging and EELS analysis of the ABAA-treated sample indicate that the increase in junction resistivity may be attributed to a more uniform barrier structure with reduced point defect density. An initial survey of the barrier thickness across each device showed no apparent difference in thickness between processed and unprocessed junctions, and the barrier remains amorphous after processing. A low-mag cross-sectional TEM/STEM image and corresponding EDS elemental distribution map are shown in Fig. 6(a-c). An amorphous a-AlO_x barrier is observed in the ABAA-treated sample (Fig. 6(d)). HAADF-STEM image shows a barrier thickness of approximately 2 nm (Fig. 6(e)).

While the ABAA technique does not appear to change the amorphous nature of the barrier from visual inspection, the chemical analysis tells a different story. We see a much more homogeneous chemistry in the ABAAtreated a-AlO_x than in untreated junctions. Our previous research showed that the distance between two main peaks labeled as A and B in Fig. 6(f-g), close to approximately 77.5 eV and 80 eV of the Al L23 energyloss near edge structure (ELNES) respectively, can be used to analyze the coordination number of Al [33–38]. Specifically, the Al L3 edges (peak A) tends to shift to higher energy as Al coordination numbers increase. For untreated junctions, a spatial variation in coordination number across the a-AlO $_x$ barrier from the untreated junction (Fig. 6(g)) [33] is demonstrated and considered as a potential decoherence source. In contrast, the ABAA-treated junction shows a uniform distribution of Al coordination number through the barrier, as the peak positions of A and B remain unchanged across the a- AlO_x layer, as shown in Fig. 6(f). This may originate from the migration/recombination of charged point defects induced by the alternating bias field [39] giving rise to a more chemically homogeneous barrier layer. This effect may increase the effective barrier height of the tunnel junction leading to the observed increase in resistance.

IV. CONCLUSION

We find that an alternating bias is effective in assisting the thermal annealing of a diatomic amorphous material, similar to adding restarts in simulated annealing solver to avoid local minima [40]. This allows for significant modifications of the junction resistance, in excess of +70%, with apparent reductions in loss and defects. The behavior of the resistance during the ABAA process showed cyclic small and large changes in resistance as the positive- and negative-bias voltages were applied and the junction resistance increased, and typically a single discontinuity in resistance was observed if sufficient number of pulses were applied. These results along with the

temperature-dependent studies and imaging point to an assisted annealing mechanism, for example, improved local ordering and/or the a-AlO $_x$ being driven into a lowerenergy glassy state[41, 42] in the potential energy landscape, as is indicated by the observed reduction in loss and TLS. In order to confirm these hypotheses, more studies such as high-resolution imaging and molecular dynamics that include density-functional theory are required. Regardless of the mechanism, we expect that a controlled alternating bias-assisted junction annealing approach will pave the way for building large-scale superconducting quantum processors by improving qubit frequency targeting, coherence, and stability. Other applications where targeting tunnel junction resistance is important may benefit by allowing for more homogeneous junction chains and ensembles for devices ranging from amplifiers to voltage standards, sensors, and data storage.

ACKNOWLEDGMENTS

The structural and chemical characterization and analysis is based upon work supported by the U.S. Department of Energy, Office of Science, National Quantum Information Science Research Centers, Superconducting Quantum Materials and Systems Center (SQMS) under contract number DE-AC02-07CH11359. We acknowledge the support of Anna Grassellino and Akshay Murthy. All resistance measurements were conducted on Form-Factor automated probe stations with the help of Anwar Aslam, Connor Smith, and Brandon Boiko. We thank Hilal Cansizoglu and the Rigetti fab team members for junction process development and samples, as well as Rory Cochrane for cryogenic measurements of transmon devices at mK temperatures. We thank Greg Stiehl for his critical eye in preparation of this manuscript.

- [1] B.D. Josephson, "Possible new effects in superconductive tunnelling," Physics Letters 1, 251–253 (1962).
- [2] J. Clarke, The SQUID handbook Vol 1 Fundamentals and technology of SQUIDs and SQUID systems (Wiley VCH, Germany, 2004).
- [3] M. H. Devoret, Quantum fluctuations in electrical circuits (Edition de Physique, France, 1997).
- [4] Y. Nakamura, Yu. A. Pashkin, and J. S. Tsai, "Coherent control of macroscopic quantum states in a single-cooperpair box," Nature 398, 786–788 (1999).
- [5] Manuel A. Castellanos-Beltran, Kent D. Irwin, Leila R. Vale, Gene C. Hilton, and Konrad W. Lehnert, "Bandwidth and dynamic range of a widely tunable josephson parametric amplifier," IEEE Transactions on Applied Superconductivity 19, 944–947 (2009).
- [6] C. Macklin, K. O'Brien, D. Hover, M. E. Schwartz, V. Bolkhovsky, X. Zhang, W. D. Oliver, and I. Siddiqi, "A near-quantum-limited josephson traveling-wave parametric amplifier," Science 350, 307-310 (2015), https://www.science.org/doi/pdf/10.1126/science.aaa8525.
- [7] K.K. Likharev and V.K. Semenov, "Rsfq logic/memory family: a new josephson-junction technology for subterahertz-clock-frequency digital systems," IEEE Transactions on Applied Superconductivity 1, 3–28 (1991).
- [8] Jian-Gang (Jimmy) Zhu and Chando Park, "Magnetic tunnel junctions," Materials Today 9, 36–45 (2006).
- [9] W. H. Rippard, A. C. Perrella, F. J. Albert, and R. A. Buhrman, "Ultrathin aluminum oxide tunnel barriers," Phys. Rev. Lett. 88, 046805 (2002).
- [10] J. J. O'Dwyer, "Current-Voltage Characteristics of Dielectric Films," Journal of Applied Physics 37, 599–601 (2004), https://pubs.aip.org/aip/jap/articlepdf/37/2/599/7938519/599_1_online.pdf.
- [11] N Cabrera and N F Mott, "Theory of the oxidation of metals," Reports on Progress in Physics 12, 163 (1949).
- [12] Xingfan Zhang, Peiru Zheng, Yingjie Ma, Yanyan Jiang, and Hui Li, "Atomic-scale understanding of oxidation

- mechanisms of materials by computational approaches: A review," Materials& Design **217**, 110605 (2022).
- [13] J. Koch, M.Y. Terri, J. Gambetta, A.A. Houck, D.I. Schuster, J. Majer, A. Blais, M.H. Devoret, S.M. Girvin, and R.J. Schoelkopf, "Charge-insensitive qubit design derived from the cooper pair box," Phys. Rev. A 76, 042319 (2007).
- [14] Charles van Duzer, Theodore; Turner, Principles of Superconductive Devices and Circuits, 2nd ed. (Prentice-Hall, Upper Saddle River NJ, 1999).
- [15] Nandini Muthusubramanian, Matvey Finkel, Pim Duivestein, Christos Zachariadis, Sean L. M. van der Meer, Hendrik M. Veen, Marc W. Beekman, Thijs Stavenga, Alessandro Bruno, and Leonardo DiCarlo, "Wafer-scale uniformity of dolan-bridge and bridgeless manhattan-style josephson junctions for superconducting quantum processors," Quantum Science and Technology (2023), 10.1088/2058-9565/ad199c.
- [16] Lunjie Zeng, Dung Trung Tran, Cheuk-Wai Tai, Gunnar Svensson, and Eva Olsson, "Atomic structure and oxygen deficiency of the ultrathin aluminium oxide barrier in Al/AlOx/Al Josephson junctions," Scientific Reports 6, 29679 (2016).
- [17] Alexander Bilmes, Alexander K Händel, Serhii Volosheniuk, Alexey V Ustinov, and Jürgen Lisenfeld, "In-situ bandaged josephson junctions for superconducting quantum processors," Superconductor Science and Technology 34, 125011 (2021).
- [18] J.M. Martinis, K.B. Cooper, R. McDermott, M. Steffen, M. Ansmann, K.D. Osborn, K. Cicak, S. Oh, D.P. Pappas, R.W. Simmonds, et al., "Decoherence in josephson qubits from dielectric loss," Phys. Rev. Lett. 95, 210503 (2005).
- [19] Steffen Schlör, Jürgen Lisenfeld, Clemens Müller, Alexander Bilmes, Andre Schneider, David P. Pappas, Alexey V. Ustinov, and Martin Weides, "Correlating decoherence in transmon qubits: Low frequency noise by

- single fluctuators," Phys. Rev. Lett. 123, 190502 (2019).
- [20] Zhijie Xu, Kevin M. Rosso, and Stephen Bruemmer, "Metal oxidation kinetics and the transition from thin to thick films," Phys. Chem. Chem. Phys. 14, 14534–14539 (2012).
- [21] Na Cai, Guangwen Zhou, Kathrin Müller, and David E. Starr, "Temperature and pressure dependent Mott potentials and their influence on self-limiting oxide film growth," Applied Physics Letters 101, 171605 (2012), https://pubs.aip.org/aip/apl/articlepdf/doi/10.1063/1.4764552/14257769/171605_1_online.pdf.
- [22] William H. Mallison, "Dependence of Critical Current Density on Oxygen Exposure in Nb-AlOx-Nb Tunnel Junctions," IEEE Transactions on Applied Superconductivity 5, 26–30 (1995).
- [23] Chang-Eun Kim, Keith G. Ray, and Vincenzo Lordi, "A density-functional theory study of the Al/AlOx/Al tunnel junction," Journal of Applied Physics 128, 155102 (2020), https://pubs.aip.org/aip/jap/articlepdf/doi/10.1063/5.0020292/14113892/155102_1_online.pdf.
- [24] M. J. Cyster, J. S. Smith, N. Vogt, G. Opletal, S. P. Russo, and J. H. Cole, "Simulating the fabrication of aluminium oxide tunnel junctions," npj Quantum Information 7, 12 (2021).
- [25] Jared B. Hertzberg, Eric J. Zhang, Sami Rosenblatt, Easwar Magesan, John A. Smolin, Jeng-Bang Yau, Vivekananda P. Adiga, Martin Sandberg, Markus Brink, Jerry M. Chow, and Jason S. Orcutt, "Laser-annealing josephson junctions for yielding scaled-up superconducting quantum processors," npj Quantum Information 7, 129 (2021).
- [26] Eric J. Zhang, Srikanth Srinivasan, Neereja Sundaresan, Daniela F. Bogorin, Yves Martin, Jared B. Hertzberg, John Timmerwilke, Emily J. Pritchett, Jeng-Bang Yau, Cindy Wang, William Landers, Eric P. Lewandowski, Adinath Narasgond, Sami Rosenblatt, George A. Keefe, Isaac Lauer, Mary Beth Rothwell, Douglas T. McClure, Oliver E. Dial, Jason S. Orcutt, Markus Brink, and Jerry M. Chow, "High-performance superconducting quantum processors via laser annealing of transmon qubits," Science Advances 8, eabi6690 (2022), https://www.science.org/doi/pdf/10.1126/sciadv.abi6690.
- [27] Hyunseong Kim, Christian Jünger, Alexis Morvan, Edward S. Barnard, William P. Livingston, M. Virginia P. Altoé, Yosep Kim, Chengyu Song, Larry Chen, John Mark Kreikebaum, D. Frank Ogletree, David I. Santiago, and Irfan Siddiqi, "Effects of laser-annealing on fixed-frequency superconducting qubits," Applied Physics Letters 121, 142601 (2022), https://pubs.aip.org/aip/apl/article-pdf/doi/10.1063/5.0102092/16484380/142601_1_online.pdf.
- [28] M. K. Konkin and J. G. Adler, "Annealing effects in tunnel junctions (voltage annealing)," Journal of Applied Physics **51**, 5450–5454 (2008), https://pubs.aip.org/aip/jap/article-pdf/51/10/5450/7969138/5450_1_online.pdf.
- [29] H. D. Ebinger and J. T. Yates, "Electron-impact-induced oxidation of Al(111) in water vapor: Relation to the Cabrera-Mott mechanism," Phys. Rev. B 57, 1976–1984 (1998).
- [30] Yide Zhang, "Magnetic annealing of magnetic alloys in a dynamic magnetic field," (2001), uS Patent 6,217,672 B1.

- [31] Noriko Yamamoto, Yamashita, and et. al, "Ultrasonic probe, piezoelectric transducer, method of manufacturing ultrasonic probe, and method of manufacturing piezoelectric transducer," (2014), uS Patent 2014/0062261 A1.
- [32] Riccardo Manenti, Eyob A. Sete, Angela Q. Chen, Shobhan Kulshreshtha, Jen-Hao Yeh, Feyza Oruc, Andrew Bestwick, Mark Field, Keith Jackson, and Stefano Poletto, "Full control of superconducting qubits with combined on-chip microwave and flux lines," Applied Physics Letters 119, 144001 (2021), https://pubs.aip.org/aip/apl/article-pdf/doi/10.1063/5.0065517/13194475/144001_1_online.pdf.
- [33] J.-S Oh, C.J. Kopas, H. Canizoglu, E. Lachman, K. Yadavalli, J.Y. Mutus, T.-H. Kim, M.J. Kramer, A.H. King, and L.) Zhou, "Correlating aluminum layer deposition rates, josephson junction microstructure, and superconducting qubits' performance," (2024), in preparation.
- [34] Danièle Bouchet and Christian Colliex, "Experimental study of elnes at grain boundaries in alumina: intergranular radiation damage effects on al-l23 and o-k edges," Ultramicroscopy **96**, 139–152 (2003).
- [35] S. Fritz, A. Seiler, L. Radtke, R. Schneider, M. Weides, G. Weiß, and D. Gerthsen, "Correlating the nanostructure of al-oxide with deposition conditions and dielectric contributions of two-level systems in perspective of superconducting quantum circuits," Scientific Reports 8 (2018), 10.1038/s41598-018-26066-4.
- [36] S. Fritz, L. Radtke, R. Schneider, M. Luysberg, M. Weides, and D. Gerthsen, "Structural and nanochemical properties of alox layers in al/alox/al-layer systems for josephson junctions," Physical Review Materials 3 (2019), 10.1103/physrevmaterials.3.114805.
- [37] K. Kimoto, Y. Matsui, T. Nabatame, T. Yasuda, T. Mizoguchi, I. Tanaka, and A. Toriumi, "Coordination and interface analysis of atomic-layer-deposition Al2O3 on Si(001) using energy-loss near-edge structures," Applied Physics Letters 83, 4306–4308 (2003), https://pubs.aip.org/aip/apl/article-pdf/83/21/4306/12229282/4306_1_online.pdf.
- [38] C Weigel, G Calas, L Cormier, L Galoisy, and G S Henderson, "High-resolution al l2, 3-edge x-ray absorption near edge structure spectra of al-containing crystals and glasses: coordination number and bonding information from edge components," Journal of Physics: Condensed Matter 20, 135219 (2008).
- [39] Mingqiang Li, Yidi Shen, Kun Luo, Qi An, Peng Gao, Penghao Xiao, and Yu Zou, "Harnessing dislocation motion using an electric field," Nature Materials 22, 958–963 (2023).
- [40] S. Alfonzetti, E. Dilettos, and N. Salerno, "Simulated annealing with restarts for the optimization of electromagnetic devices," IEEE Transactions on Magnetics 42, 1115–1118 (2006).
- [41] Hideki Hashimoto, Yohei Onodera, Shuta Tahara, Shinji Kohara, Koji Yazawa, Hiroyo Segawa, Motohiko Murakami, and Koji Ohara, "Structure of alumina glass," Scientific Reports 12, 516 (2022).
- [42] Pablo G. Debenedetti and Frank H. Stillinger, "Supercooled liquids and the glass transition," Nature 410, 259–267 (2001).